# Numerical Exposure Assessment Report

 $SAR-NS\_FCC-ISED-CE\_6220312\_Charger-3\_V1.5$ 

Customer: Boston Scientific Corporation

Document Version 1.5 / 19th Nov, 2024

Author: David Schäfer

IMST GmbH Carl-Friedrich-Gauß-Str. 2–4 47475 Kamp-Lintfort Germany



# **Numerical Exposure Assessment Report**

Versions <sup>1</sup>				
Release Date	Nr.	Author	Comments	
22nd Jul, 2022	1.0	David Schäfer	Initial version	
9th Feb, 2023	1.1	David Schäfer	Used new reference measurements for DUT with updated firmware (cf sec. 2.2.4)	
20th Mar, 2023	1.2	David Schäfer	More info for coil geometry, model uncertainty/validation and frequency scaling.	
29th Jun, 2023	1.3	David Schäfer	Check larger phantom-DUT-gaps (cf sec. 3.4)	
29th Jun, 2023	1.4	David Schäfer	Refined mesh for gap-simulations	
19th Nov, 2024 1.5 David Schäfer		David Schäfer	Added accreditation info, technical drawing, detailed depiction of the excitation port, tabular data for the H-field lines, explanation+results for passive receiver at shallow implantation depth and updated RSS-102 reference from Issue 5 to 6	

Approval					
Name	Job Title	Date	Signature		
David Schäfer	Preparation	19th Nov, 2024	0-5/1		
Jens Lerner	Review	19th Nov, 2024	Jens Your		

Laboratory						
Name and Address	IMST GmbH	IMST GmbH, Test Center				
	Carl-Friedri	ch-Gauß-Str. 2–4				
	47475 Kam	47475 Kamp-Lintfort				
Accreditation	DAKS Doutsche Akrediterungsstelle D-PL-12139-01-00	The Testcenter at IMST GmbH is a conformity assessment body (CAB) accredited by the German Accreditation Body "Deutsche Akkreditierungsstelle GmbH" (DAkkS), registered at D-PL-12139-01-00 and according to the accreditation scope D-PL-12139-01-02. It is a designated testing laboratory by the German Federal Network Agency				
	BNetzA-CAB-24/21-23	for Electricity, Gas, Telecommunications, Post and Railway" Bundes-netzagentur" (BNetzA), registered at BNetzA-CAB-24/21-23.				

Customer (Applicant / Manufacturer)					
Name and Address	Boston Scientific Corporation	Same as applicant			
	25155 Rye Canyon Loop				
	CA91355 Valencia, United States				
	Contact: Javad Paknahad				

<sup>&</sup>lt;sup>1</sup>A new report revision replaces all previous versions, which hence become invalid.



Device Under Test (DUT)				
Type of DUT	Wireless Power Transfer Charger			
Model Name	Charger 3			
FCC ID	Q4D-SC5314			
ISED Cert. No.	9773A-SC5314			
ISED HVIN	SC5314			
Frequency Band	81 kHz			
Active Elements	one coil			

# **Evaluation Results**

		Below exposure limit set by				
Quantity inside flat phantom	Result*	ICNIRP 2020	47 CFR § 1.1310	RSS-102 Issue 5	1999/ 519/EC	RPS S-1
EIAV <sub>max</sub>	8.5643 V/m			Yes		Yes

<sup>\*</sup> Simulated values for "reported model", cf. section 3.2

<sup>\*\*</sup> Not applicable combinations were indicated as "—"

# **Human Exposure Limits**

# Specific Absorption Rate (ICNIRP [1], 1999/519/EC [2], RPS S-1 [3])

	Uncontroll	ed Environment	Controlled Environment	
Condition	(Gene	eral Public)	(Occupational)	
	SAR Limit	Mass Avg.	SAR Limit	Mass Avg.
SAR averaged over the whole body mass	0.08 W/kg	whole body	0.4 W/kg	whole body
Peak spatially-averaged SAR for the head, neck & trunk	2.0 W/kg	10 g of tissue*	10 W/kg	10 g of tissue*
Peak spatially-averaged SAR in the limbs/extremities	4.0 W/kg	10 g of tissue*	20 W/kg	10 g of tissue*
*: Defined as a tissue volume in the shape of a cube				

## Specific Absorption Rate (RSS-102 Issue 5 [4], RSS-102 Issue 6 [5])

	Uncontroll	ed Environment	Controlled Environment	
Condition	(General Public)		(Occupational)	
	SAR Limit	Mass Avg.	SAR Limit	Mass Avg.
SAR averaged over the whole body mass	0.08 W/kg	whole body	$0.4\mathrm{W/kg}$	whole body
Peak spatially-averaged SAR for the head, neck & trunk	1.6 W/kg	1 g of tissue*	8 W/kg	1 g of tissue*
Peak spatially-averaged SAR in the limbs/extremities	4.0 W/kg	10 g of tissue*	20 W/kg	10 g of tissue*
*: Defined as a tissue volume in the shape of a cube				

# Specific Absorption Rate (47 CFR Ch. I § 1.1310 [6])

	Uncontroll	ed Environment	Controlled Environment	
Condition	(Gene	eral Public)	(Occupational)	
	SAR Limit	Mass Avg.	SAR Limit	Mass Avg.
SAR averaged over the whole body mass	0.08 W/kg	whole body	0.4 W/kg	whole body
Peak spatially-averaged SAR	1.6 W/kg	1 g of tissue*	8 W/kg	1 g of tissue*
Peak spatially-averaged SAR for extremities, such as hands, wrists, feet, ankles, and pinnae	4.0 W/kg	10 g of tissue*	20 W/kg	10 g of tissue*
*: Defined as a tissue volume in the shape of a cube				

# Internal Electric Field (ICNIRP [1], RSS-102 Issue 5 [4], RSS-102 Issue 6 [5])

	Uncontrolled Environment	<b>Controlled Environment</b>	
Condition	(General Public)	(Occupational)	
	EIAV Limit	EIAV Limit	
Peak EIAV @ f (in Hz)	$1.35\cdot 10^{-4}\cdot f \text{ V/m}$	$2.7\cdot 10^{-4}\cdot f \text{ V/m}$	
Peak EIAV @ 81 kHz	10.935 V/m	21.87 V/m	

# Frequency Scopes

	9					
Regulation	local	whole body	EIAV			
ICNIRP	$100\mathrm{kHz} - 6\mathrm{GHz}$	$100\mathrm{kHz} - 300\mathrm{GHz}$	$100\mathrm{kHz} - 10\mathrm{MHz}$			
47 CFR § 1.1310	100 kH:	*				
RSS-102 Issue 5	100 kH:	$3\mathrm{kHz} - 10\mathrm{MHz}$				
RSS-102 Issue 6	100 kH:	$3\mathrm{kHz} - 10\mathrm{MHz}$				
1999/ 519/EC	100 kHz	_				
RPS S-1	$100\mathrm{kHz} - 6\mathrm{GHz}$ $100\mathrm{kHz} - 300\mathrm{GHz}$		$100\mathrm{kHz} - 10\mathrm{MHz}$			
*: Not applicable combinations were indicated as "—"						

# **Contents**

1	Intro	oduction	7
	1.1	Objective	7
	1.2	Simulation Method	7
	1.3	DUT Description	7
	1.4	Setup for Reference Measurement	7
2	EM :	Simulation Model	10
	2.1	Model Setup	10
	2.2	Model Check	13
		2.2.1 Magnetic Fields	13
		2.2.2 Coil Inductance	13
		2.2.3 Conclusion of Model Check	15
		2.2.4 Statement on Report Revision 1.1	15
3	EIA\	' Evaluation	17
	3.1	Simulation Results	18
	3.2	Simulation Uncertainty	18
		3.2.1 Simulation Parameter Related Uncertainty	18
		3.2.2 Model Related Uncertainty	20
		3.2.3 Model Validation	21
		3.2.4 Uncertainty Budget	22
		3.2.5 Uncertainty Penalty	22
	3.3	Passive Receiver Impact	22
	3.4	Impact of larger Phantom-DUT-Gaps	25
	3.5	Conclusion of EIAV Evaluation	26
4	Арр	endix	27
	4.1	Specific Information for Computational Modelling	27
	4.2	Abbreviations	28
5	Refe	erences	29
Li	st o	f Figures	
	1	Photo of the DUT	8
	2	Technical drawing of the DUT	8
	3	Measurement setup CTC	9

	4	Geometry of the model - outer	10
	5	Geometry of the model - internal	11
	6	Geometry of the model - exploded	12
	7	Magnetic field plane	13
	8	Line evaluation, graph	15
	9	Geometry of the phantom	17
	10	Simulated EIAV results	18
	11	Geometry of the passive receiver dummy	23
	12	EIAV for the model with the passive receiver dummy	23
	13	EIAV with the passive receiver dummy in non-typical setup	24
	14	Influence of 5 mm gap on EIAV	25
	15	Influence of 25 mm gap on EIAV	25
Li	st o	f Tables	
	1	Tabular data of the measurement results shown in Figure 8 and the simulation results evaluated at the measurement locations up to a distance of $45\mathrm{mm.}$	14
	2	Measured and simulated inductance	15
	3	The applicants description of the different DUT firmware versions, used for the h-field reference measurements	16
	4	EIAV maximum value	18
	5	Uncertainty Budget Procedure	19
	6	EIAV results for different phantom positions	19
	7	EIAV results for different mesh resolutions	19
	8	EIAV results for different simulation domain sizes	19
	9	EIAV results for different number of total time steps	20
	10	EIAV results with and without frequency scaling	20
	11	Uncertainty budget, simulation parameters, EIAV	20
	12	Uncertainty budget, model setup	21
	13	Combined and expanded uncertainty, EIAV	22
	14	Influence of passive receiver dummy on EIAV	23
	16	Influence of larger gaps on EIAV	25
			~ ~



#### Introduction 1

#### 1.1 Objective

The objective is the numerical exposure assessment of a Wireless Power Transfer (WPT) charger (further referred to as "device under test" or "DUT") designed by Boston Scientific Corporation (further referred to as "applicant"). In particular the internal electric field (EIAV<sup>2</sup>, instantaneous nerve stimulation hazard) was investigated and compared to the exposure limits specified by ISED [5, 7] and the ARPANSA [3].

#### Simulation Method 1.2

All simulations were done with the Finite Difference Time Domain (FDTD) simulation tool Empire XPU [8]. A numerical model of the DUT was generated and validated by measurements of the magnetic field in its vicinity and measured inductance of the charging coil. The EIAV inside a flat phantom (human body part model) was investigated similar to the assessment procedures described in IEC/IEEE 62704-1 [9, 10]. The procedures were adapted to make them suitable for the low frequency of the DUT.

#### 1.3 **DUT Description**

The WPT charger "Charger 3" (further referred to as "device under test" or "DUT") features a single charging coil, operates at 81 kHz and is intended to charge medical implants called "internal pulse generators" ("IPG", also produced by the applicant). During charging the DUT is placed directly on the human skin. Photos of the DUT are depicted in Figure 1 and a technical drawing including the DUTs dimensions is shown in Figure 2.

#### Setup for Reference Measurement 1.4

A validation of the numerical model was carried out by comparing the simulated magnetic field in the vicinity of the DUT with a reference measurement. The measurement was done on the behalf of the applicant by the lab of "CTC advanced GmbH" with the setup depicted in Figure 3. They used a "DASY8" positioner system from Speag and a "MAGPy-H3D" magnetic field probe with a 1 cm<sup>2</sup> sensor size (loop) and 6.6 mm sensor center to tip distance. The measurements were done for a series production equivalent device Model SC-5314, running in a testing operating mode at a fixed coil current of  $1.65\,\mathrm{A}$  (RMS). The applicant pre-determined this to be the maximum expectable coil current during charging an WPT receiver (IPG). No WPT receiver was present during the reference measurements of the magnetic field.

For the reference measurement the field probe was located directly above the xy-center of the coil. A line measurement of the magnetic field strength was performed by lifting the probe upwards along the coil axis to different z-distances from the DUT. Figure 3 (a) shows the lowest possible position of the field probe (touch position).

<sup>&</sup>lt;sup>2</sup>EIAV is the particular name of the post-processing/visualisation feature in Empire XPU. The averaging is optional and was disabled for this investigation.



Figure 1: Photo of the DUT

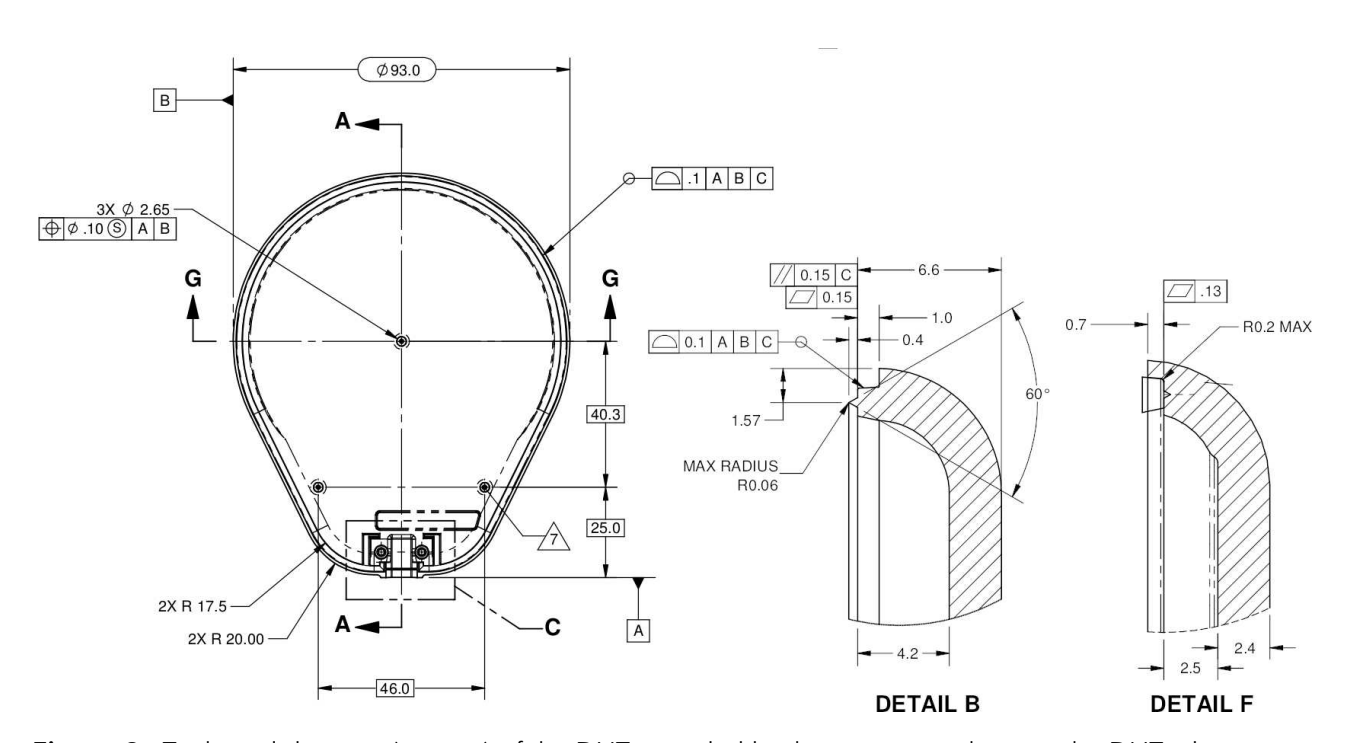


Figure 2: Technical drawing (excerpt) of the DUT provided by the customer, showing the DUTs dimensions in top view as well as details in side view.

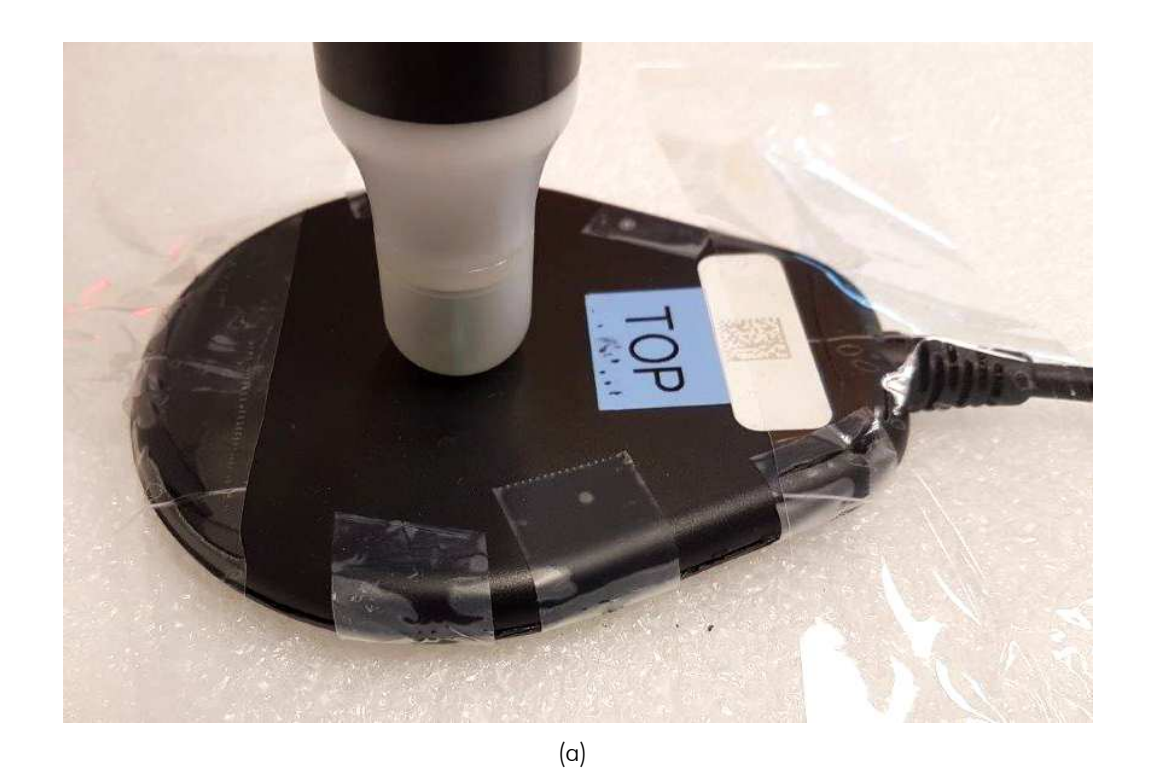




Figure 3: Measurement setup from the external lab of "CTC advanced GmbH", showing (a) a close-up of the "MAGPy-H3D" probe in touch position and (b) the "DASY8" positioner.

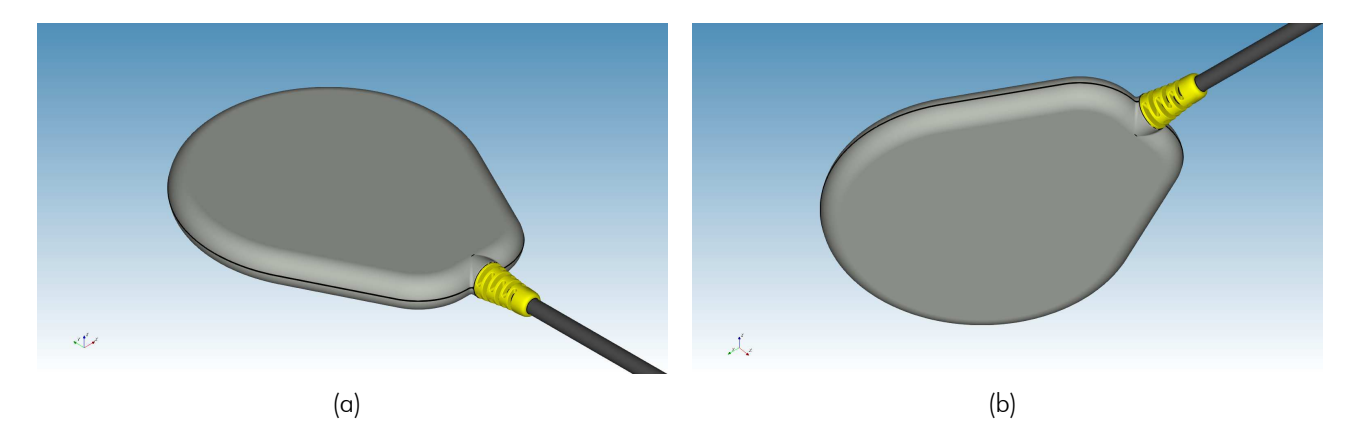
## 2 EM Simulation Model

## 2.1 Model Setup

The simulation model of the DUT is based on STEP CAD data, technical drawings and photos provided by the applicant. First the CAD data was imported into Empire XPU and then the missing coil geometry was modelled. The coil consists of 3 layers of 9 turns, so of a total of 27 coil windings. Turns are staggered to increase tightness. After the coil was modelled, it was reviewed together with the applicant to ensure the numerical coil is in sufficient agreement with the actual device coil. Some principally unavoidable differences exist as listed below. Their impact will later be quantified in the calculation of the model related uncertainty (cf. section 3.2.2).

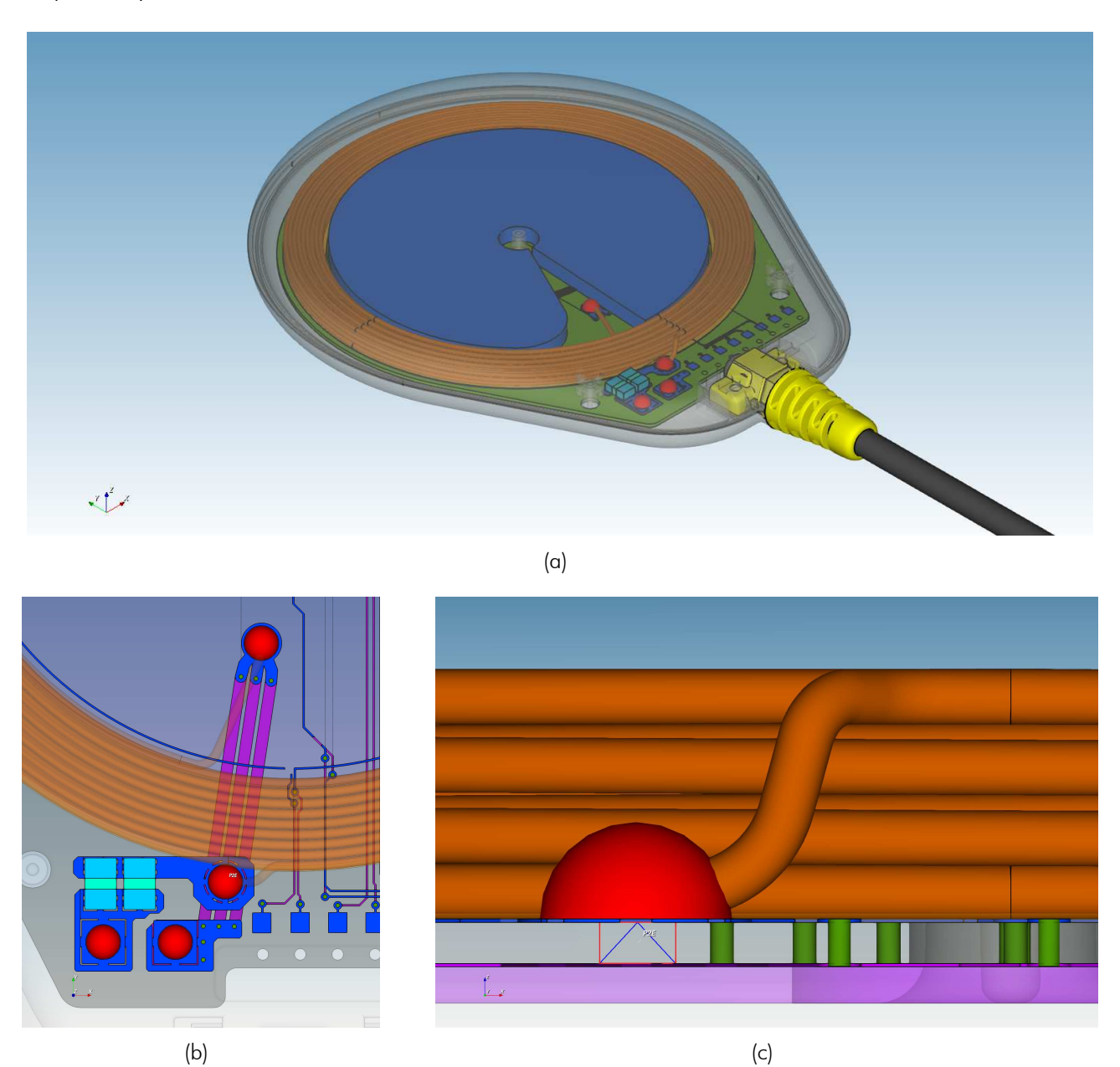
- The actual coil consists of tightly packed multistrand wire (Litz wire) with very thin isolating coating between turns/layers. The numerical coil needs to consist of a thin singlestrand wire with sufficiently large gaps between turns/layers to prevent short circuits in the discretised structure. By comparison with simplified analytical calculations it can be shown that this is a legitimate simplification.
- 2. The technical drawing of the coil states certain tolerances for the coils dimensions. Correspondingly there are differences in coil dimension between the actual/hardware DUT and the numerical model as well as between different (hardware) DUT samples.

The geometrical center of the coil was chosen as the coordinate origin of the numerical model. Figure 4 shows a top and bottom 3D view of the simulation model.



**Figure 4**: Geometry of the Empire simulation model of the DUT, showing the outer view on the top (a) and bottom (b) side.

In Figure 5 the internal components can be seen, including the WPT charging coil (brown) located in the middle of the device being wrapped around a dielectric thermal diffuser (blue). The top side of the charging coil and the DUT housing are located at  $z=1.37\,\mathrm{mm}$  and  $z=5.75\,\mathrm{mm}$  respectively.



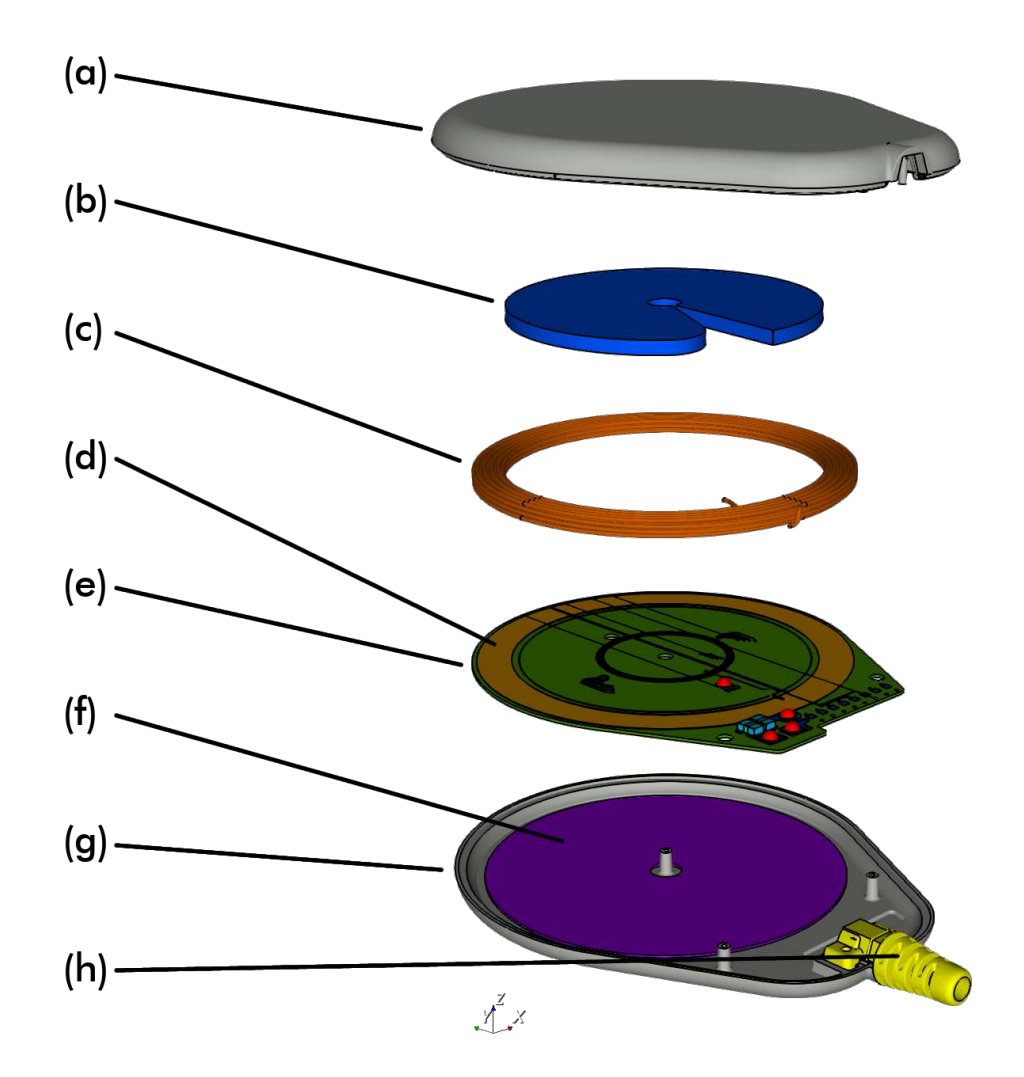
**Figure 5**: Geometry of the Empire simulation model of the DUT. The housing of the DUT is set transparent to show the internal components (a). The excitation port was attached between the top and bottom layer of the PCB, i.e. between the location of the outer coil soldering pad and a bottom side trace connected to the inner coil soldering pad (b).

Figure 6 shows an exploded view of the most important components of the simulation model. Based on the applicants information the material properties were set as follows:

(a) Top housing (Dielectric,  $\varepsilon_r=2.25$  ,  $tan(\delta)=0.01$  )



- (b) Thermal diffuser (Dielectric,  $\varepsilon_r = 2.25$  ,  $tan(\delta) = 0.01$  )
- (c) WPT coil (Copper,  $\sigma = 58 \cdot 10^6 \, \text{S/m}$ )
- (d) WPT coil adhesive (Dielectric,  $\varepsilon_r=2.25$  ,  $tan(\delta)=0.01$  )
- (e) PCB FR4 substrate (Dielectric,  $\varepsilon_r=4.9$  ,  $tan(\delta)=0.025$  )
- (f) PCB adhesive (Dielectric,  $\varepsilon_r=2.25$  ,  $tan(\delta)=0.01$ )
- (g) Bottom housing (Dielectric,  $\varepsilon_r=2.25$  ,  $tan(\delta)=0.01$  )
- (h) Cable strain relief (Dielectric,  $\varepsilon_r=2.25$  ,  $tan(\delta)=0.01$  )



**Figure 6**: Geometry of the Empire simulation model of the DUT, showing an exploded view of the top housing (a), the thermal diffuser (b), the WPT coil (c), WPT coil adhesive (d), PCB FR4 substrate (e), PCB adhesive (f), bottom housing (g) and the cable strain relief (h).

## 2.2 Model Check

The simulation model was checked by comparing the simulated magnetic fields with the reference measurement (cf. section 1.4). During measurement the WPT coil was excited with the maximum expectable current of  $1.65\,\mathrm{A}$  (RMS) at a frequency of  $81\,\mathrm{kHz}$ . The simulation setup was unperturbed, meaning that it didn't include a WPT receiver device or phantom (human body model).

## 2.2.1 Magnetic Fields

Figure 7 shows a xz-cutplane for the simulated magnetic field strength through the center of the DUT. The colour legend is logarithmic with an 70 dB range. It can be seen how the magnetic field is mostly unperturbed by the PCB and therefore symmetric in x- and z-direction.

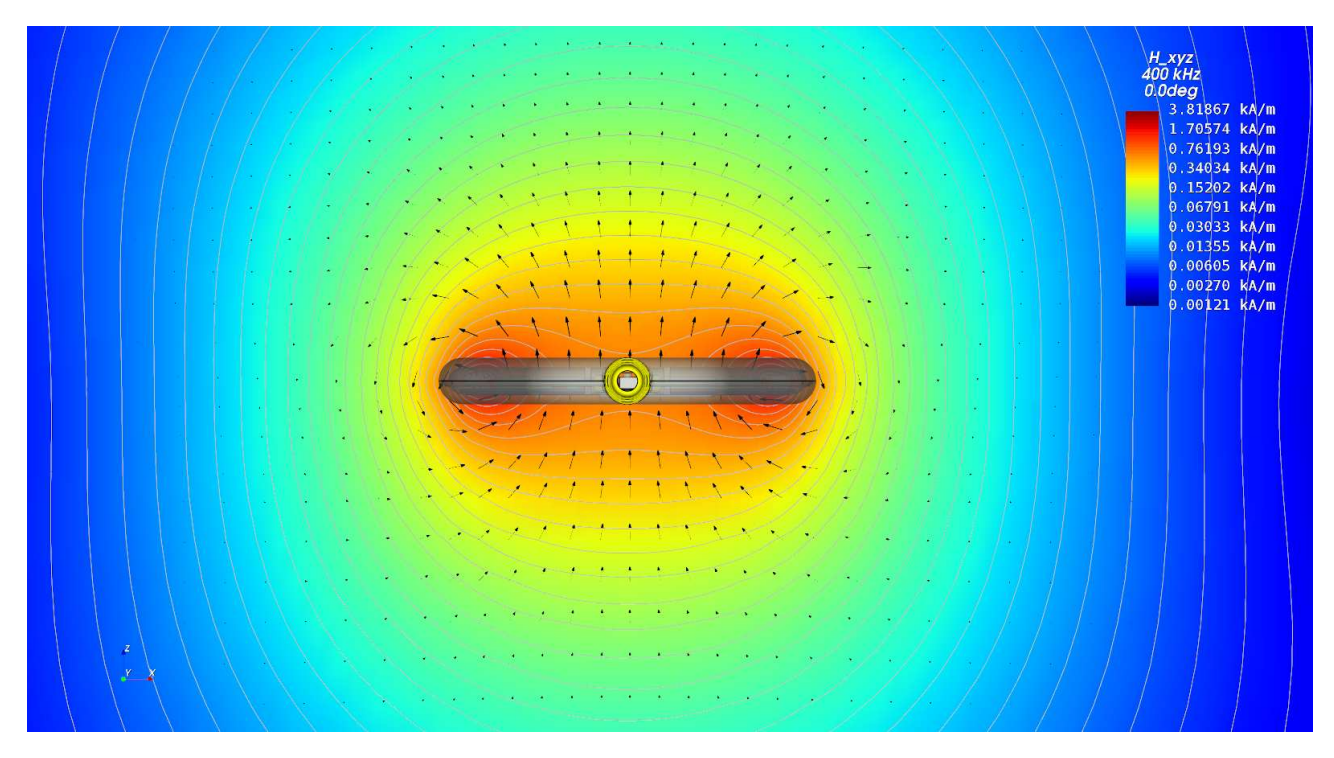


Figure 7: The simulated magnetic field displayed on a xz-plane through the DUT.

Analogue to the setup of the measurement (cf. section 1.4) the simulated magnetic field (H-field) strength was evaluated along the axis of the coil. The measurements start at  $z=5.75\,\mathrm{mm}+7\,\mathrm{mm}=12.75\,\mathrm{mm}$ , whereby 7 mm approximately corresponds to the "sensor center to tip distance" of the "MAGPy-H3D" field probe. The simulated line starts at  $z=0\,\mathrm{mm}$  which is  $5.75\,\mathrm{mm}$  below the top of the DUTs housing.

As Table 1 and Figure 8 show, the simulated H-field is in good agreement with the top-side measurement, showing a deviation of only  $1.47\,\%$  at the probes touch position. For the bottom-side measurement the deviation is slightly larger with  $5.46\,\%$  at the probes touch position.

#### 2.2.2 Coil Inductance

In addition to the magnetic fields also the inductance of the coil was used to check the simulation model. The measured value was taken from the data sheet of the coil module provided by the

	Measurement	Measurement	
z (mm)	Top (A/m)	Bottom (A/m)	Empire (A/m)
12.8	514.650	536.420	507.108
13.8	500.640	522.460	494.133
14.8	486.470	508.130	480.788
15.8	472.040	493.380	467.106
16.8	457.490	478.770	453.284
17.8	442.870	463.850	439.376
18.8	428.420	448.740	425.418
19.8	413.900	433.830	411.479
20.8	399.380	419.290	397.647
21.8	385.250	404.620	383.941
22.8	371.270	390.190	370.391
23.8	357.440	376.120	357.185
24.8	344.020	362.180	344.136
25.8	330.980	348.630	331.312
26.8	318.050	335.530	319.003
27.8	305.770	322.640	306.982
28.8	293.800	309.970	295.180
29.8	282.110	297.960	283.751
30.8	270.920	286.140	272.850
31.8	260.020	274.720	262.201
32.8	249.480	263.720	251.778
33.8	239.600	253.040	241.995
34.8	229.810	242.900	232.516
35.8	220.410	233.050	223.315
36.8	211.510	223.470	214.512
37.8	202.840	214.390	205.998
38.8	194.580	205.715	197.955
39.8	186.720	197.360	190.117
40.8	179.140	189.418	182.533
41.8	172.030	181.769	175.510
42.8	165.240	174.384	168.695
43.8	158.630	167.467	162.062
44.8	152.380	160.787	155.765
45.8	146.420	154.385	149.818

Table 1: Tabular data of the measurement results shown in Figure 8 and the simulation results evaluated at the measurement locations up to a distance of  $45\,\mathrm{mm}$ .



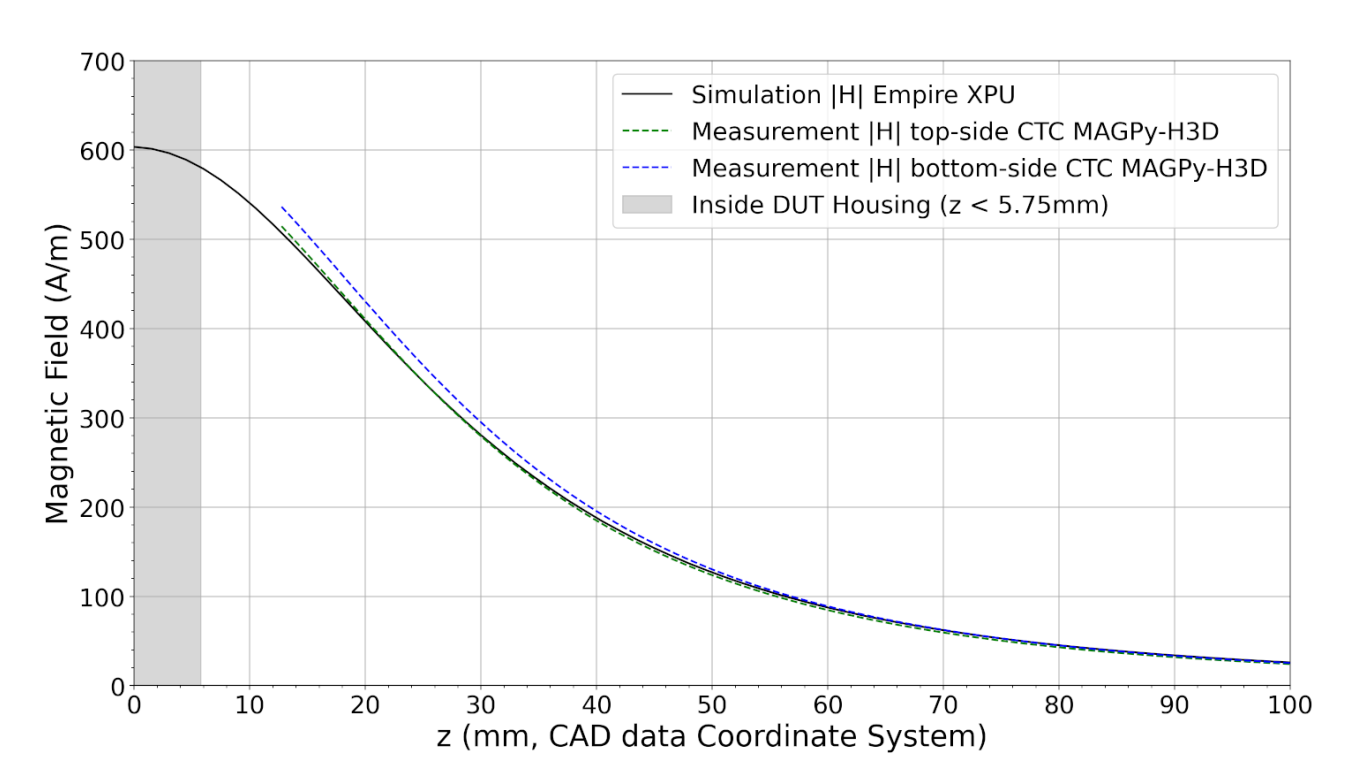


**Figure 8**: Curves for the line evaluation of the H-field (RMS values). The top of the DUT dielectric housing is located at  $z=5.75\,\mathrm{mm}$ .

applicant. With a relative deviation of  $6.76\,\%$  (cf. Table 2) the simulated inductance is in good agreement with the measurement.

	Measured	<b>Empire</b>	Deviation
Coil Inductance	94.50 <i>μ</i> Η	$100.89 \mu H$	6.76%

**Table 2**: Measured and simulated inductance.

### 2.2.3 Conclusion of Model Check

It can be concluded, that simulated magnetic field strength and inductance are in good agreement (cf. Figure 8 and Table 2) with the measurements from the applicant and the external lab of "CTC advanced GmbH", indicating the accurate setup of the numerical simulation model.

#### 2.2.4 Statement on Report Revision 1.1

The reference measurement data used for the initial report version 1.0 was in good agreement with the simulation for larger distances, but showed a substantial difference in the close range. The cause of the deviation was investigated considering various possible reasons, but at first no explanation could be found. Therefore an uncertainty penalty was added, the initial report 1.0 was handed in to ISED, but got rejected. After further investigations by the applicant it could be determined that apparently there was a change in coil current as reaction to the presence of the measurement probe. For revision 1.1 of the report the reference measurements were repeated



with a new firmware which is optimized for a more stable coil current. A description of the two DUT firmware versions by the applicant can be found in table 3.

DUT firmware	Description
9028485-EMI-f2 (report 1.0)	"Directly sets fixed charging frequency (sets power depending how close it is to resonance) and duty cycle in test firmware, chosen to match the highest power level corresponding to maximum misaligned IPG at maximum charge depth when using the App FW."
9028484-000-b0 (report 1.1)	"Dynamically adjusts charging frequency to find resonance, duty cycle is adjusted based on feedback from the sense coil voltage. This approach exactly replicates the highest power level by setting the target sense coil voltage to the fixed level corresponding to the use case of maximum misaligned IPG at maximum charge depth when using the App FW."

**Table 3**: The applicants description of the different DUT firmware versions, used for the h-field reference measurements

The initial reference measurement data showed almost equal magnetic fields for the top- and bottom-side measurements, whereby the top-side fields were slightly stronger. In the new measurement data, the fields for the bottom-side were stronger and in less good agreement with the simulation (cf. Figure 8). Therefore the bottom-side measurement data was used as reference for the calculation of the model related uncertainty, to follow the conservative worst-case approach.

## 3 EIAV Evaluation

For the evaluation of the internal Electric field (EIAV) a box shaped flat phantom was added to the simulation model. The setup resembles the situation of the DUT being placed onto the body at a location where no IPG is implanted, which is expected to be the worst case scenario $^3$ . The continuous maximum expectable coil current of  $1.65\,\mathrm{A}$  (RMS) was retained throughout the investigation.

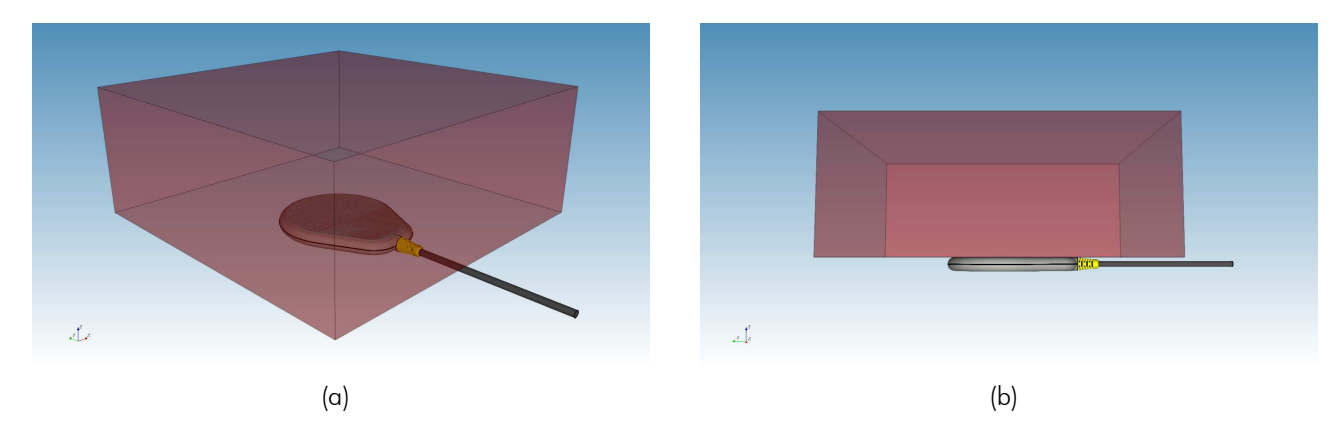


**Figure 9:** Geometry of the flat phantom in 3D view (a) and side view (b) showing it is in touch with the DUTs housing.

The phantom was centred (xy-direction) above the active coil at closest possible z-distance, virtually touching the top side of the DUT dielectric housing as shown in Figure 9. With respect to the CAD coordinate system origin, the phantoms bottom side (side towards DUT) is located at  $z=5.75\,\mathrm{mm}$ . The dimensions and the material properties of the phantom are as follows:

- 1. Geometric Size:  $d_x \cdot d_y \cdot d_z = 250\,\mathrm{mm} \cdot 250\,\mathrm{mm} \cdot 100\,\mathrm{mm}$
- 2. Relative Permittivity:  $\epsilon_r = 55$
- 3. Electrical Conductivity:  $\sigma = 0.75\,\mathrm{S/m}$
- 4. Mass Density:  $\rho = 1000\,\mathrm{kg/m^3} = 1\,\mathrm{g/cm^3}$

To decrease simulation time, the results were evaluated at  $f=400\,\mathrm{kHz}$  and scaled to the DUTs operating frequency of  $f=81\,\mathrm{kHz}$  using an algorithm originally proposed by O.P. Gandhi [11, sec. 46.5]. More details about the numerical model, like e.g. domain size, time step or total number of mesh cells, can be found in the appendix in section 4.1.



<sup>&</sup>lt;sup>3</sup>This assumption will be investigated in section 3.3.

## 3.1 Simulation Results

Figure 10 shows the simulated un-averaged EIAV and Table 4 lists the corresponding maximum value and its position.

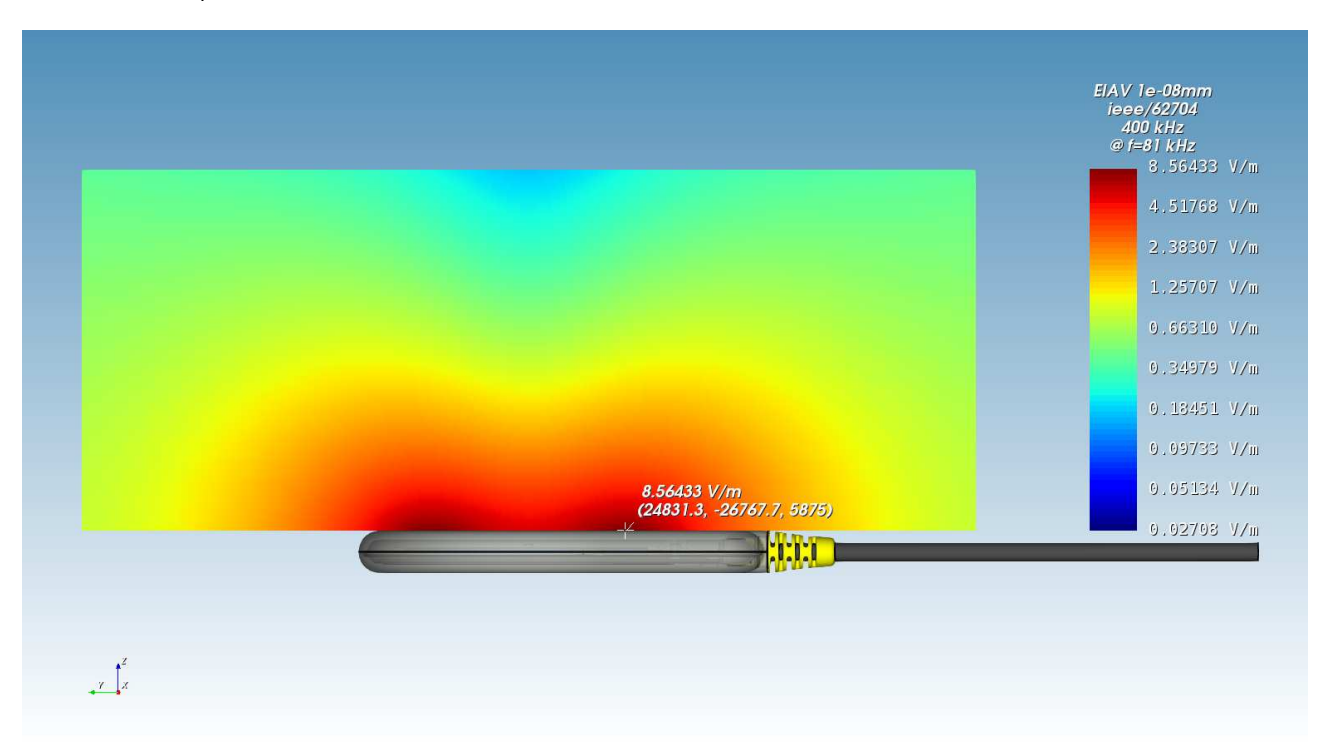


**Figure 10**: Cutplane through the maximum of the simulated EIAV inside the flat phantom. The phantom geometry is not visible.

	Maximum	Position of Maximum		
Quantity	Value	x y		z
EIAV <sub>unaveraged,max</sub>	$8.56433\mathrm{V/m}$	$24.8313\mathrm{mm}$	$-26.7677\mathrm{mm}$	$5.875\mathrm{mm}$

**Table 4**: EIAV maximum value with its corresponding position.

## 3.2 Simulation Uncertainty

Based on chapter 7 of IEC/IEEE 62704-1 [9] the Combined- and Expanded Standard Uncertainty was calculated to analyse the accuracy of the results for the numerical model (further referred to as "reported model"). Because the DUTs operating frequency is below the scope of the standard, the procedure had to be modified. Details about this will be described in the following sections.

## 3.2.1 Simulation Parameter Related Uncertainty

The procedure for evaluating the simulation parameter related uncertainty (IEC/IEEE 62704-1 [9, section 7.2]) was modified as described in Table 5. The Tables 6, 7, 8, 9 and 10 show the maximum EIAV for the investigated variants as well as their relative deviation from the reported model. Table 11 shows the budget of the EIAV uncertainty contributions of the simulation parameters.

Uncertainty Component	Applicability of the Procedure from IEC/IEEE 62704-1 [9, section 7.2]	Nr. of Vari- ations
Positioning	Applicable. Variation will be: Increase of distance between phantom and DUT by +1 mesh step	1
Mesh Resolution	Not 1:1 applicable. Requested refinement is not practicable at 81 kHz. Instead, total number of mesh cells will be increased by a factor of 2	1
Boundary Condition	Not 1:1 applicable, because $\lambda/4 @ 81  \mathrm{kHz} = 925  \mathrm{m}$ is way too large. Instead, simulation domain will be enlarged by 50% simultaneously in $+/-  \mathrm{x/y/z}$ direction	1
Power Budget	Not applicable. No travelling wave conditions are given, so comparison with power absorbed in ABC is not possible. Excitation will be normalized to fixed port/coil current.	0
Convergence	Not 1:1 applicable. Instead, variation will be simulated longer by a factor of 1.5 or more.	1
Phantom dielec- trics	Not applicable / not indicated because fixed permittivity and conductivity from IEC/TR 62905 were used.	0
Frequency scal- ing	Frequency scaling based on O.P. Gandhi algorithm [11, sec. 46.5]. This uncertainty component is not contained in the standard and was considered with normal probability distribution (conservative, rectangular distribution may as well be justified).	1

**Table 5**: Description of the modified procedure for obtaining the uncertainty budget.

Phantom z-Position	5.75 mm	$6.00\mathrm{mm}$
EIAV <sub>max</sub>	$8.56433\mathrm{V/m}$	$8.3963\mathrm{V/m}$
EIAV-Deviation	0 %	-1.962%

**Table 6**: EIAV results for different phantom positions. The first data column corresponds to the reported model (cf. section 3.1).

Mesh Resolution	10.1 MCells	$23.6\mathrm{MCells}$
EIAV <sub>max</sub>	$8.56433\mathrm{V/m}$	$8.5756\mathrm{V/m}$
EIAV-Deviation	0 %	0.131%

**Table 7:** EIAV results for different mesh resolutions. The first data column corresponds to the reported model (cf. section 3.1).

Domain Size	$450 \cdot 450 \cdot 436.465\mathrm{mm}$	$900 \cdot 900 \cdot 872.93\mathrm{mm}$		
EIAV <sub>max</sub>	$8.56433\mathrm{V/m}$	$8.5619\mathrm{V/m}$		
EIAV-Deviation	0 %	-0.029%		

**Table 8**: EIAV results for different simulation domain sizes. The first data column corresponds to the reported model (cf. section 3.1). The simulation domain was enlarged symmetrically in all spatial directions.

Time/Convergence	$30\mathrm{Msteps}$	$45\mathrm{Msteps}$		
Energy Decay	$-76.7338\mathrm{dB}$	$-79.6148\mathrm{dB}$		
EIAV <sub>max</sub>	$8.56433\mathrm{V/m}$	$8.5481\mathrm{V/m}$		
EIAV-Deviation	0 %	-0.189%		

**Table 9:** EIAV results for different number of total time steps. The first data column corresponds to the reported model (cf. section 3.1).

Native Frequency	400 kHz	81 kHz	
Time/Convergence	$30\mathrm{Msteps}$	$30\mathrm{Msteps}$	
EIAV <sub>max</sub>	$8.56433\mathrm{V/m}$	$8.5533\mathrm{V/m}$	
EIAV-Deviation	0 %	-0.129%	

**Table 10**: EIAV results with and without frequency scaling based on O.P. Gandhi algorithm [11, sec. 46.5]. The first data column corresponds to the reported model (cf. section 3.1).

Uncertainty Component	Section in [9]	EIAV Toler- ance in %	Probability Distribution	Divisor	$c_i$	EIAV Uncer- tainty in %
Positioning	7.2.1	-1.962%	R	1.73	1	-1.134%
Mesh Resolu- tion	7.2.2	0.131 %	N	1	1	0.131 %
Boundary Condition	7.2.3	-0.029%	N	1	1	-0.029%
Power Budget	7.2.4	not appl.	Z	1	1	not appl.
Convergence	7.2.5	-0.189%	R	1.73	1	-0.109%
Phantom dielectrics	7.2.6	not appl.	R	1.73	1	not appl.
Frequency scaling	-	-0.129%	N	1	1	-0.129%
Combined Std.	1.155%					

**Table 11**: Budget of the EIAV uncertainty contributions of the simulation parameters, analogue to the budget of the SAR uncertainty contributions of the simulation parameters to IEC/IEEE 62704-1 [9, Table 3]. Note: N, R, U = normal, rectangular, U-shaped probability distributions.

#### 3.2.2 Model Related Uncertainty

For distances  $d < \lambda/2$  the IEC/IEEE 62704-1 [9, section 7.3.3] states that "[...] the only way to determine the uncertainty of the DUT model is by SAR measurements", which is not possible for the given frequency of the DUT. Therefore the procedure was modified by using the squared H-field values instead of SAR/EIAV in [9, equation 14], similar to the assessment for distances  $d \geq \lambda/2$  by [9, equation 13]. The bottom-side measurement data was used as reference, as explained in section 2.2.4.



$$U_{\rm sim,model} = max \left( \frac{|H_{\rm ref,n}^2 - H_{\rm sim,n}^2|}{H_{\rm ref,max}^2} \right) \tag{1} \label{eq:Usim,model}$$

$$= \left[ \frac{|(536.42\,\text{A/m})^2 - (507.11\,\text{A/m})^2|}{(536.42\,\text{A/m})^2} \right]_{z=12.75\,\text{mm}}$$
(2)

$$=10.630\%$$
 (3)

Table 12 shows the budget of the uncertainty contributions of the model parameter. The applicant stated an k=2 uncertainty of  $1.24\,\mathrm{dB} \Rightarrow 15.28\,\%$  for the measurements done by CTC advanced (cf. section 1.4), so 7.673% was used for the k=1 uncertainty of the measurement equipment and procedure.

Uncertainty Component	Section in [9]	Tolerance in %	Probability Distribution	Divisor	$c_i$	Uncer- tainty in %
Uncertainty of the DUT model	7.3.2 or 7.3.3	10.630%	N	1	1	$\boxed{10.630\%}$
Uncertainty of the phantom model	7.3.3	not appl.	N	1	1	not appl.
Uncertainty of the measurement equipment and procedure	-	7.673 %	N	1	1	7.673 %
Combined Std. Uncertainty (k=1)			13.110%			

Table 12: Budget of the uncertainty contributions of the model setup, corresponding to IEC/IEEE 62704-1 [9, Table 4]. Note: N, R, U = normal, rectangular, U-shaped probability distributions.

#### 3.2.3 Model Validation

To validate the numerical model, equation 15 from IEC/IEEE 62704-1 [9, section 7.3.4] was calculated for the H-field line evaluation:

$$E_{n} = max \left( \sqrt{\frac{(\nu_{\text{sim,n}} - \nu_{\text{ref,n}})^{2}}{(\nu_{\text{sim,n}} U_{\text{sim}(k=2)})^{2} + (\nu_{\text{ref,n}} U_{\text{ref}(k=2)})^{2}}} \right)$$
(4)

$$= max \left( \sqrt{\frac{(H_{\text{sim,n}}^2 - H_{\text{ref,n}}^2)^2}{(H_{\text{sim,n}}^2 U_{\text{sim}(k=2)})^2 + (H_{\text{ref,n}}^2 U_{\text{ref}(k=2)})^2}} \right)$$
 (5)

$$\begin{split} E_n &= max \left( \sqrt{\frac{(\nu_{\text{sim,n}} - \nu_{\text{ref,n}})^2}{(\nu_{\text{sim,n}} U_{\text{sim}(k=2)})^2 + (\nu_{\text{ref,n}} U_{\text{ref}(k=2)})^2}} \right) \\ &= max \left( \sqrt{\frac{(H_{\text{sim,n}}^2 - H_{\text{ref,n}}^2)^2}{(H_{\text{sim,n}}^2 U_{\text{sim}(k=2)})^2 + (H_{\text{ref,n}}^2 U_{\text{ref}(k=2)})^2}} \right) \\ &= \left[ \sqrt{\frac{((507.11\,\text{A/m})^2 - (536.42\,\text{A/m})^2)^2}{((507.11\,\text{A/m})^2 \cdot (21.261\,\%))^2 + ((536.42\,\text{A/m})^2 \cdot (15.345\,\%))^2}} \, \right]_{z=12.75\,\text{mm}} \end{split} \tag{6}$$

$$=0.435 \le 1$$
 (7)

The condition/inequation is fulfilled, indicating that the deviation is within the expected uncertainty, and hence that the model is valid.

## 3.2.4 Uncertainty Budget

The budgets for simulation parameters related uncertainties and model related uncertainties were combined (k=1) and expanded (k=2) for EIAV as shown in table 13.

Uncertainty Component	Section in [9]	Tolerance in %	Probability Distribution	Divisor	$c_i$	Uncer- tainty in %
Uncertainty of the DUT model with respect to simulation parameters	7.2	1.155%	N	1	1	1.155%
Uncertainty of the developed numerical model of the DUT	7.3	13.110 %	N	1	1	13.110%
Combined Std. Uncertainty (k=1)			13.161%			
Expanded Std. Uncertainty (k=2)			26.321%			

**Table 13**: Combined and expanded budget of the EIAV uncertainty, analogue to the budget of the SAR uncertainty from IEC/IEEE 62704-1 [9, Table 5]. Note: N, R, U = normal, rectangular, U-shaped probability distributions.

#### 3.2.5 Uncertainty Penalty

The calculated Expanded Std. Uncertainties for SAR/EIAV do not exceed the maximum of  $30\,\%$ stated in IEC/IEEE 62704-1 [9, Section 7.4]. Therefore uncertainty penalties as described in EN 62311 [12, Section 6.2, Equation 1] were not applied.

#### 3.3 Passive Receiver Impact

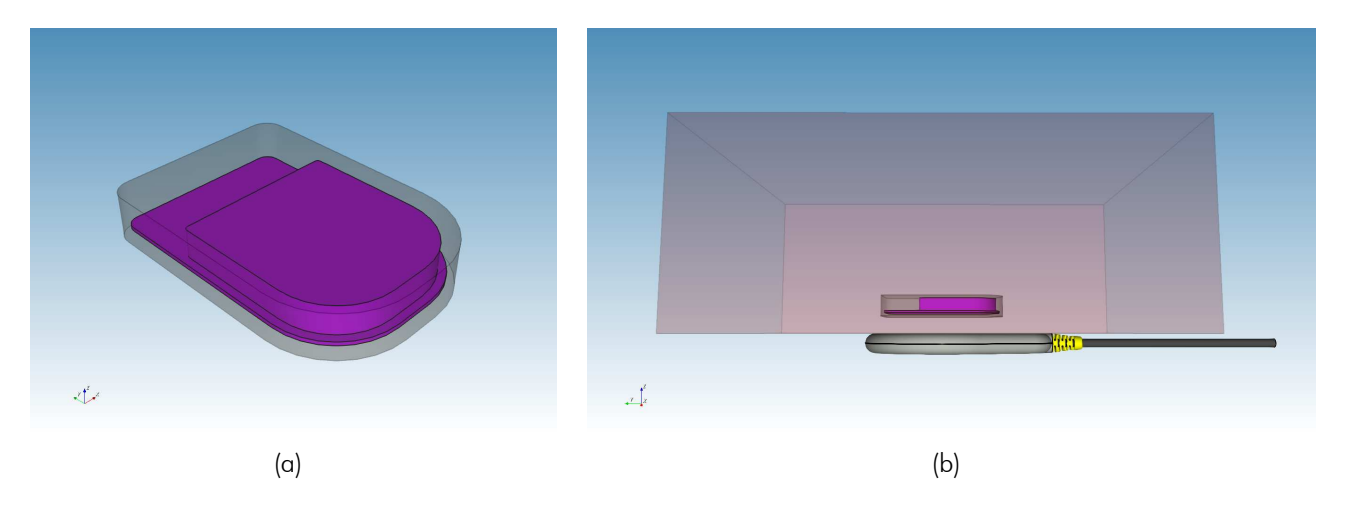
During the intended use of the DUT, a WPT receiver (IPG) is implanted in the human body at the location where the DUT is placed onto the skin. However, in the reported model there was no receiver present, expecting this situation to be the worst case exposure scenario. As an empirical test, a simplified passive receiver dummy was added to the numerical model as shown in Figure 11. It consists of a dielectric housing (transparent gray) and copper parts (purple) and was placed inside the phantom at a distance of 10 mm from its bottom surface.

Table 14 compares the maximum values for EIAV and their position for the model without and with the passive receiver dummy. Figure 12 shows the corresponding EIAV distribution. The maximum EIAV is lower than in case of the reported model, which is in consistence with Lenz's law: The induced currents in the dummy receiver generate a magnetic field that opposes the changes in the initial magnetic field from the DUT. Therefore the superimposed total H-field is weakened and the EIAV is decreased.



Quantity	Reported Model	With Passive Receiver
EIAV <sub>unaveraged,max</sub>	$8.56433\mathrm{V/m}$	$7.51481\mathrm{V/m}$

**Table 14**: EIAV maximum value for the model with the passive receiver dummy.



**Figure 11**: Geometry of the passive receiver dummy, consisting of a dielectric housing with bounding box dimensions of  $46 \cdot 68 \cdot 8.45$  mm and a copper plate inside (a). The receiver dummy was placed within the phantom at a distance of 10 mm from the phantoms lower surface (b).

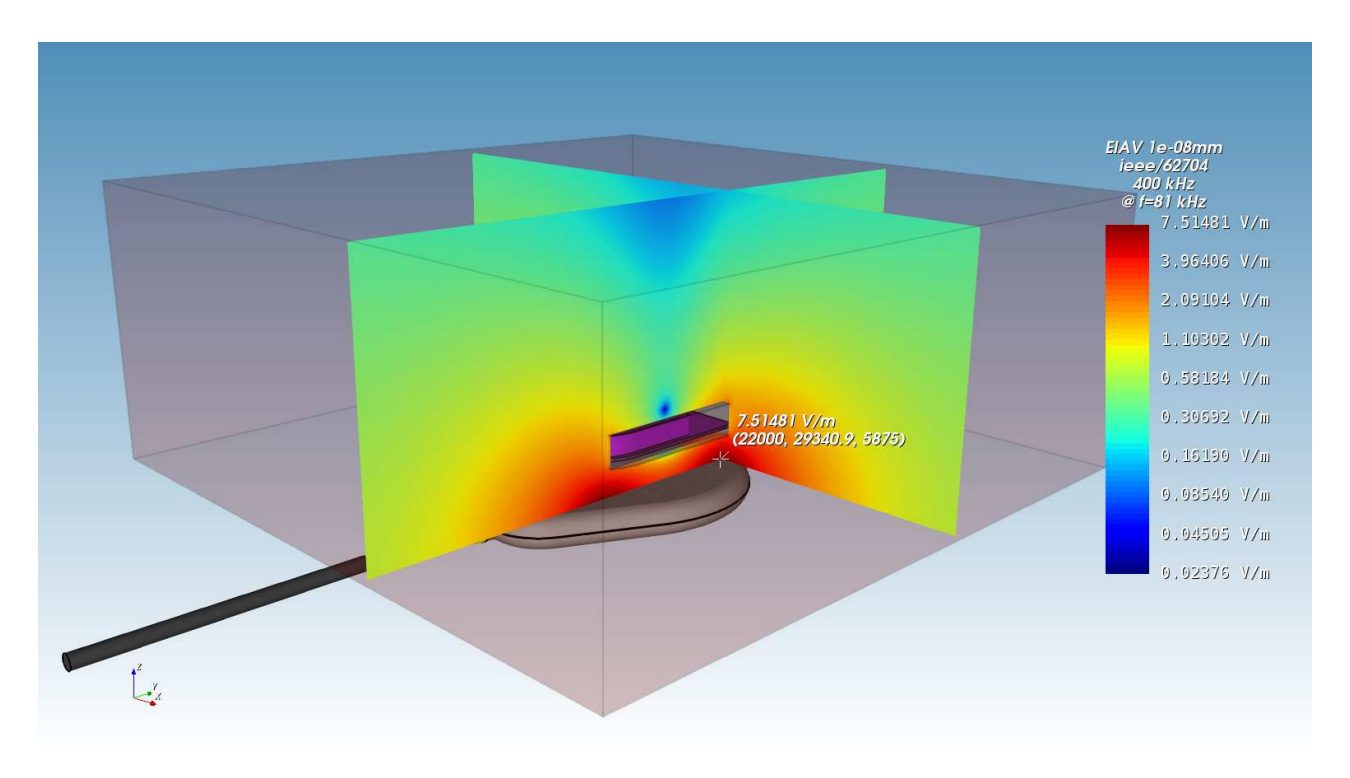


**Figure 12:** Cutplane through the maximum of the simulated EIAV inside the flat phantom for the model with the passive receiver dummy.

A moderate increase of exposure may occur in case of non-typical shallow implantation depths of less than 10 mm in combination with a sideward (x-/y-direction) shift of the receiver dummy. Under this conditions the replacement of the tissue by the dummies dielectric housing effectively changes the shape of the phantom to such an extend, that the path of the currents induced in the phantom becomes locally narrowed at the dummy location.

Figure 13 shows the EIAV distribution for an implantation depth of 5 mm, which the customer indicated as the extremest case that can happen. The sideward shift of the receiver dummy in this case was -37 mm in x-direction. As shown in Table 15 the before mentioned effect increases the exposure compared to the typical receiver location (implantation depth of 10 mm, centered above DUT), but in this particular case it is still lower than for the reported model.

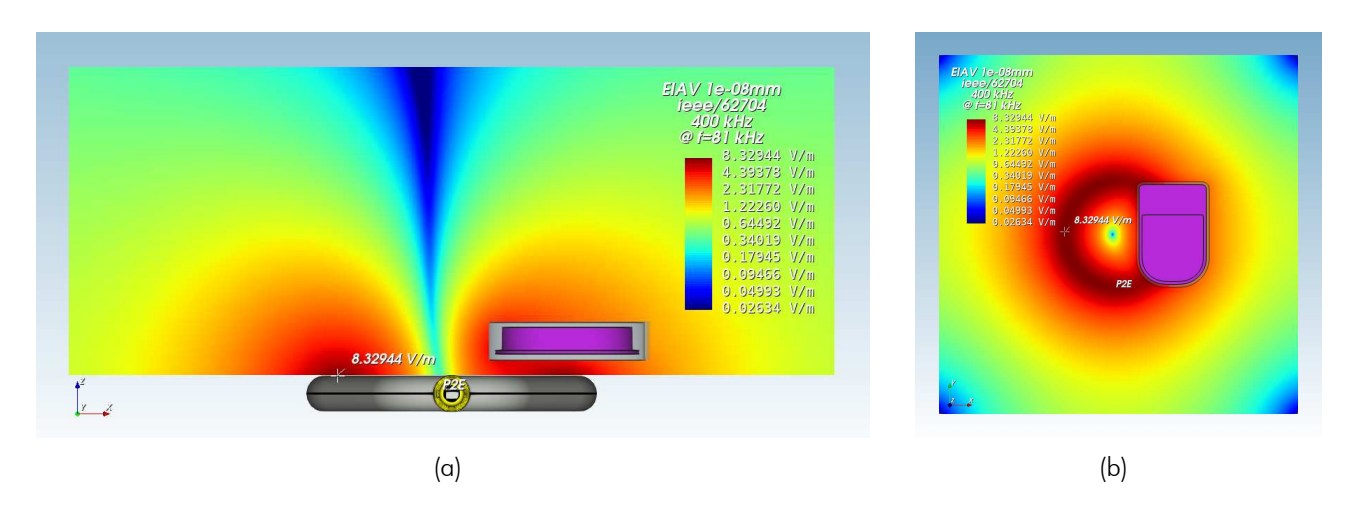


**Figure 13:** Cutplane through the maximum of the simulated EIAV inside the homogeneous phantom for the model with the passive receiver dummy at non-typical shallow implantation depth of  $5 \, \text{mm}$  and an x-direction shift of  $-37 \, \text{mm}$ .

Quantity	Reported Model	With Passive Receiver at non-typical 5 mm Implantation Depth
EIAV <sub>unaveraged,max</sub>	$8.56433\mathrm{V/m}$	$8.32944\mathrm{V/m}$

**Table 15**: EIAV maximum values for the model with the passive receiver dummy at non-typical shallow implantation depth of 5 mm and an x-direction shift of -37 mm.

## Impact of larger Phantom-DUT-Gaps

The influence of a small gab between DUT and phantom on the exposure was quantified during the calculation of the simulation parameter related uncertainty (cf. section 3.2.1 and IEC/IEEE 62704-1 [9, section 7.2.2]). Additionally also the impact of larger gaps of 5 mm and 25 mm was investigated to confirm that the reported model resembles the worst-case scenario. To improve the comparability of the results the mesh at the phantoms bottom side was refined to match the local resolution of the reported model.

Quantity	Reported Model	5 mm Gap	25 mm Gap
EIAV <sub>unaveraged,max</sub>	$8.56433\mathrm{V/m}$	$6.05818\mathrm{V/m}$	$2.30306\mathrm{V/m}$

Table 16: Influence of larger gabs between DUT and phantom on EIAV.

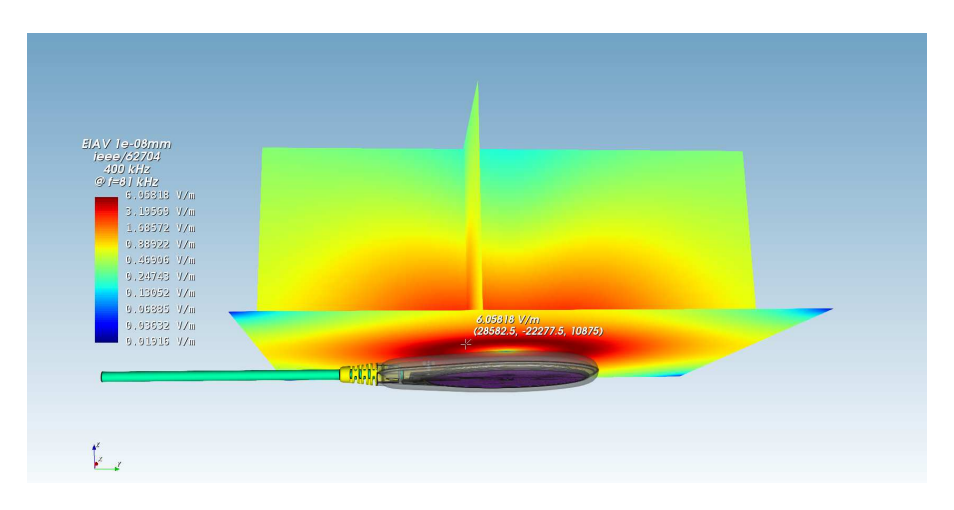


Figure 14: Influence of 5 mm gap between DUT and phantom on EIAV.

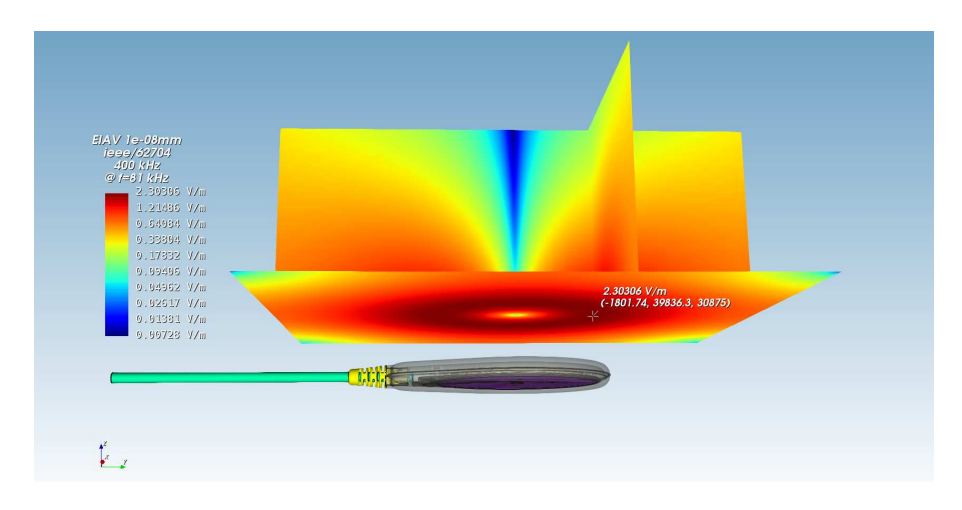


Figure 15: Influence of 25 mm gap between DUT and phantom on EIAV.

Table 16, Figure 14 and Figure 15 show that a larger gap significantly reduces the maximum ElAV. This is because the continuous maximum expectable coil current of  $1.65\,\mathrm{A}$  (RMS) was retained throughout the investigation, and therefore larger gaps only result in weaker H-fields and EIAV inside the phantom.

## 3.5 Conclusion of EIAV Evaluation

Summarizing the numerical exposure assessment of the DUT, the following can be stated:

- 1. The simulated magnetic field strength and the coil inductance are in good agreement with the measurements (cf. section 2.2), indicating the accurate setup of the DUT simulation model (without phantom).
- 2. The investigated scenario (reported model) follows the worst-case assumption that:
  - (a) The flat phantom is in direct contact with the DUT with no implanted receiver present.
  - (b) The DUT is exciting its coil with the maximum expectable current, despite the fact that no receiver device is present.
  - (c) The search mode duty cycle is neglected.
- 3. The model validation (cf. section 3.2.3) shows that in-equation 15 from IEC/IEEE 62704-1 is fulfilled, indicating a valid numerical model.
- 4. The uncertainty analysis shows an Expanded Standard Uncertainty of  $U_{\mathsf{sim}(\mathsf{k}=2)} = 26.321\,\%$  for EIAV (cf. section 3.2.4), which is below the permissible 30% stated in IEC/IEEE 62704-1 section 7.4.
- 5. The evaluated maximum EIAV (internal Electric field) is  $8.56433\,\mathrm{V/m}$ .
- 6. With respect to the statements above, the conclusion of this numerical exposure assessment report is, that the DUT does <u>not</u> exceed the EIAV exposure limits specified by ISED [5, 7] and ARPANSA [3]. A tabular evaluation can be found at the beginning of the report.



# **Appendix**

#### 4.1 Specific Information for Computational Modelling

Computational resources Computation was performed on an Intel Xeon Platinum 816824-core processor with 1.319 GB memory usage.

**FDTD** algorithm implementation and validation cf. [10]

Computational parameters for reported model:

**Cell Size (min/max)**: 0.1777 mm / 10.37 mm

**Domain Size:**  $450 \cdot 450 \cdot 436.465 \, \text{mm}$ 

**Total amount of mesh cells:** approx. 10.1 million

Time step:  $2.03999 \cdot 10^{-13}$  s

Total number of time steps: approx. 30 million **Simulation time:** approx. 5 hours and 58 minutes

**Simulation speed:** 14383 million cells per second (14.383 GCells/s) **Excitation method:** Gaussian pulse with  $f_0 = 0 \, \text{Hz}$ ,  $f_{\text{BW}} = 4 \, \text{MHz}$ 

**Postprocessing:** Results were evaluated at  $f = 400 \, \text{kHz}$  and scaled to DUT operating fre-

quency of f = 81 kHz using O.P. Gandhi algorithm [11, sec. 46.5].

Phantom model implementation cf. section 3

**Tissue dielectric parameters** cf. section 3

**Transmitter model implementation and validation** cf. section 2

Test device positioning cf. section 3

Steady state termination procedures A Gaussian pulse was used for the excitation and the simulation was terminated after the energy had dissipated to more than  $-76.7338\,\mathrm{dB}$ .

Test results cf. section 3



## 4.2 Abbreviations

Abbreviation	Description	
CAD	Computer Aided Design	
DUT	Device Under Test	
EIAV	Averaged Internal Electric Field	
EM	Electro Magnetic	
FDTD	Finite Difference Time Domain	
PCB	Printed Circuit Board	
RF	Radio Frequency	
RMS	Root Mean Square	
SAR	Specific Absorption Rate	
S/m	Siemens per meter = $1/(\Omega m)$	

**Table 17**: Abbreviations.

#### 5 References

- [1] International Commission on Non-Ionizing Radiation Protection (ICNIRP), "ICNIRP Guidelines for limitting Exposure to Electromagnetic Fields (100 KHz to 300 GHz)," 2020.
- [2] European Council, "Council Recommendation of 12 July 1999 on the limitation of exposure of the general public to electromagnetic fields (0 Hz to 300 GHz), 1999/519/EC," July 1999.
- [3] Australian Radiation Protection and Nuclear Safety Agency (ARPANSA), "Standard for Limiting Exposure to Radiofrequency Fields – 100 kHz to 300 GHz - Radiation Protection Series S-1, RPS S-1," February 2021.
- [4] Innovation, Science and Economic Development Canada (ISED, Canada), "RSS-102 Issue 5 - Radio Freguency (RF) Exposure Compliance of Radiocommunication Apparatus (All Frequency Bands), with Amendment 1 from February 2, 2021," March 2015.
- [5] —, "RSS-102 Issue 6 Radio Frequency (RF) Exposure Compliance of Radiocommunication Apparatus (All Frequency Bands)," December 2023.
- [6] Federal Communications Commission (FCC, USA), "FCC Limits for Specific Absorption Rate (SAR), 47 C.F.R. § 2.1093," 2012.
- [7] Innovation, Science and Economic Development Canada (ISED, Canada), "RSS-102.NS.SIM Issue 1 - Simulation Procedure for Assessing Nerve Stimulation (NS) Compliance in Accordance with RSS-102," December 2023.
- [8] IMST GmbH. (2022, August) Empire XPU. Carl-Friedrich-Gauß-Str. 2-4, 47475 Kamp-Lintfort, Germany. [Online]. Available: http://empire.de
- [9] "IEC/IEEE International Standard Determining the peak spatial-average specific absorption rate (SAR) in the human body from wireless communications devices, 30 MHz to 6 GHz - Part 1: General requirements for using the finite-difference time-domain (FDTD) method for SAR calculations," IEC/IEEE 62704-1:2017, pp. 1-86, 2017.
- [10] IMST GmbH, "EMPIRE XPU Code Verification according to IEC/IEEE P62704-1."
- [11] —, EMPIRE XPU Manual, October 2021.
- [12] CENELEC, "Assessment of electronic and electrical equipment related to human exposure restrictions for electromagnetic fields (0 Hz to 300 GHz), EN IEC 62311," January 2020.

